# *Proposal of Self-Excited Wound-Field Magnetic Geared Motor for HEV Application*

Masahiro Aoyama, and Yoshihisa Kubota
Shizuoka University / SUZUKI Motor Corporation
300 Takatsuka-cho, Minami-ku, Hamamatsu,
Shizuoka 432-8611, Japan
aoyamam@hhq.suzuki.co.jp
kubotay@hhq.suzuki.co.jp

Toshihiko Noguchi
Shizuoka University
3-5-1 Johoku, Naka-ku, Hamamatsu,
Shizuoka 432-8561, Japan
noguchi.toshihiko@shizuoka.ac.jp

***Abstract*—This paper describes a permanent-magnet-free magnetic geared motor where magnetic flux variation in differencial frequency between stator rotating magnetic field and rotor rotation speed is effectively utilized for field magnetization instead of permanent magnets. The operation principle of the self-excitation with diode rectifier on rotor winding circuit is discussed in this paper. Magnetic circuit design and structural design of downsized prototype machine were performed for the purpose of verification of the self-excitation principle. In addition, the adjustable speed drive characteristics of proposed motor are investigated by FE analysis.**

***Keywords—magnetic geared motor; wound-field; differencial frequency; collinear chart; self-excitation; diode rectifier; HEV***

## I. INTRODUCTION

A sustainable transportation system can be achieved through the development of higher-efficiency vehicles with significantly lower fuel consumption [1]. Recently, the new standards are achievable effectively with electrified powertrains utilizing electric propulsion motors [2]-[5]. Electric motors have much higher efficiencies than an ICEs and, thus, require less energy. Interior PM Synchronous Machines (IPMSM) are employed in the most of the currently available hybrid and electric vehicles on the market, including the TOYOTA Prius (motor 60 kW, generator 42 kW), CHEVY Volt (motor 110 kW, generator 55 kW), and NISSAN Leaf (80 kW) [6]-[8]. With the use of high-energy and high-coercivity, competing well against other motor technologies, i.e., induction machine, switched reluctance machine. In addition, differing from battery powered electric vehicles (EVs) such as NISSAN Leaf, HEVs involve two energy sources, namely the gasoline and the battery, as well as two propulsion devices, namely the engine and the motor. Their key challenge is how to effectively combine the engine driving force and the motor driving force in such a way that the engine can always operate at its optimal efficiency and produce the minimum tailpipe exhaust. The existing HEVs essentially adopt the same technology, termed the planetary-geared electronic-continuously variable transmission (E-CVT) propulsion system, to combine the engine driving force and the motor driving force. However, this system suffers from the drawbacks of low power density, high transmission loss, wear-and tear problem and annoying audible noise. Rather than using physical contacts to perform force transmission as adopted by mechanical gears, flux modulated type magnetic gears can transmit the force using contactless magnetic attraction [9]-[17]. The use of coaxial arrangement can further enable magnetic gears to simultaneously utilize magnets for force transmission. By purposely designing the modulating ring of the magnetic gear to be rotationable, it can work as the planetary gear for power splitting HEVs, e.g., Toyota-Hybrid-System-II (THS-II) employed for TOYOTA Prius. The engine power flow can be split into two paths, one path is via the outer rotor (Modulator) of the magnetic gear while another path is via the inner rotor (PM-rotor) of the magnetic gear. Increasingly, both the motor and the generator can be integrated into the magnetic gear to form a single machine unit. On one side of such the advantages, conventional magnetic-geared motor has a serious problem. Rare-earth sintered magnets with high energy product are selected for permanent magnets (PMs) used in magnetic gear. However, since rare-earth sintered PMs have high electric conductivity (not as strong as metals such as copper though), eddy current will occur in the PM and become the cause for decrease in transfer efficiency of magnetic gear and for demagnetization of PM. Eddy current of PMs will occur due to variations on magnetic flux density in air gap, however, due to the principle of magnetic gears using pole pieces, the magnetic flux density distribution of gaps have various harmonic components, including even the asynchronous frequency between a rotating magnetic field of stator and the PM-rotor. In addition, a large quantity of expensive magnets are used due to couple with the magnetism of PMs.

To solve these problems, a novel self-excited wound-field magnetic geared motor is proposed in this paper. Wound-field rotor (WF-rotor) that replace the PMs with electromagnets are consist of self-excited technologies applied diode rectifier circuit utilizing magnetic flux variation in differencial frequency between stator and rotor (differencial frequency magnetic flux) as replacement of the PM-rotor [18]-[20]. Actually, the self-excited technique is not required to inject/withdraw currents into/from the rotating rotor windings

978-1-4673-7151-3/15/$31.00 ©2015 IEEE

with slip ring. Theoretical analysis of the proposed motor is developed and analytically explained in the discussion that the differencial frequency magnetic flux can be mainly retrieved for the field magnetization with diode rectifier circuit. The operation characteristics of the proposed motor are analytically investigated through the electromagnetic field analysis with computer simulation.

## II. Operation Principle of Proposed Motor

### A. Conventional PM-type

A cross section diagram of the conventional motor (PM-rotor) and HEV system application is shown in Fig. 1. Because, dual-axis drive is possible as shown in Fig. 1 (b), a collinear chart of Fig. 2 are satisfied. Where, $\omega_s$ is the angular velocity of stator rotating magnetic field, $\omega_m$ is the angular velocity of PM-rotor, $\omega_{pm}$ is the angular velocity of PM-rotor, $P_s$ is the stator pole-pair, $P_{pm}$ is the PM-rotor pole pair and $P_m$ is the modulator pole, respectively. Since dual-axis drive is possible, collinear chart relation is composed of outer rotor (Modulator) attached to the final driveline (Drive shaft) and inner rotor (PM-rotor) connected to the engine shaft for HEV system. The gear ratio is determined by a pole combination. Here, the armature magnetomotive force $F_s(\theta, t)$ can be expressed as:

$$f_s(\theta,t) = f_{ac}\sin\{P_s(\theta-\omega_s t)\}, \tag{1}$$

where $f_{ac}$ is a amplitude of armature magnetomotive force, and armature magnetomotive force is approximately sinusoidal waveform. Then, the spatial permeance distribution of modulator $P(\theta, t)$ is given by Eq. (2) with approximated sinusoidal waveform, similarly.

$$P(\theta,t) = \lambda_{dc} + \lambda_{ac}\sin\{P_m(\theta-\omega_m t)\}, \tag{2}$$

where $\lambda_{dc}$ is the constant parts, and $\lambda_{ac}$ is the amplitude of the periodical variations. Thus, magnetic flux distribution in air gap $\phi(\theta, t)$ is obtained by the vector product between Eq. (1) and Eq. (2):

$$\begin{aligned}\phi(\theta,t) &= f_s(\theta,t)\times P(\theta,t)\\ &= f_{ac}\lambda_{dc}\sin\{P_s(\theta-\omega_s t)\}\\ &+\frac{1}{2}f_{ac}\lambda_{ac}\cos\left\{(P_m-P_s)(\theta-\frac{-P_s}{P_m-P_s}\omega_s t-\frac{P_m}{P_m-P_s}\omega_m t)\right\}\\ &+\frac{1}{2}f_{ac}\lambda_{ac}\cos\left\{(P_m+P_s)(\theta-\frac{P_s}{P_m+P_s}\omega_s t-\frac{P_m}{P_m+P_s}\omega_m t)\right\}\end{aligned} \tag{3}$$

As expressed in the above expression, the magnetic flux in air gap is composed of the three different rotating magnetic field, i.e., the first term is the pole-pair $P_s$ in stator fundamental frequency, the second and the third term corresponds to the pole-pair ($P_m$ - $P_s$) and ($P_m$ + $P_s$). The angular velocities $\omega_{pm}$, $\omega'_{pm}$ in the second and third term are expressed as

$$\omega_{pm} = -\frac{P_s}{P_m-P_s}\omega_s + \frac{P_m}{P_m-P_s}\omega_m \tag{4}$$

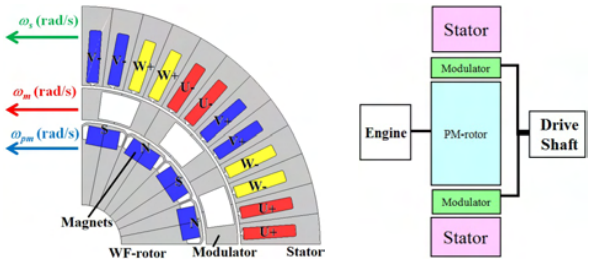


(a) Conventional magnetic geared motor. (b) HEV system.

Fig. 1. Cross section of conventional magnetic geared motor and HEV system application.

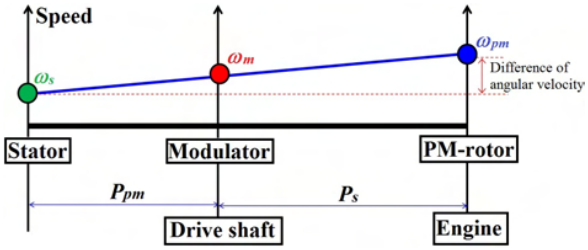


Fig. 2. Collinear chart applied magnetic geared motor for HEV system.

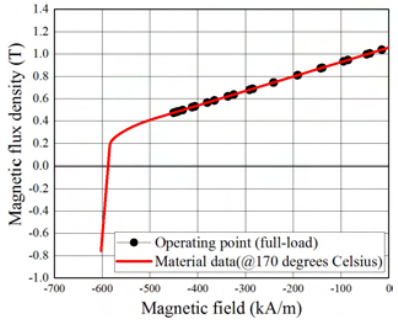


Fig. 3. Operating point of magnet permeance under full-load.

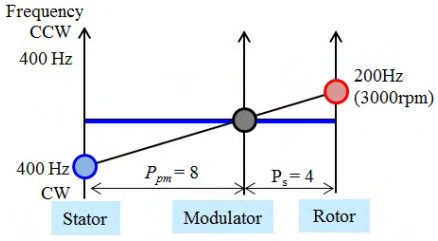


Fig. 4. Operating condition for FEA.

$$\omega'_{pm} = -\frac{P_s}{P_m+P_s}\omega_s + \frac{P_m}{P_m+P_s}\omega_m \tag{5}$$

Thus, the PM-rotor and the modulator can be simultaneously rotated with satisfying the following relationship:

$$P_m\omega_m \pm P_{pm}\omega_{pm} = P_s\omega_s\,. \tag{6}$$

The magnetic permeability of the air gap reluctance generally decreases with respect to frequency increase so that it is common to apply the following pair:

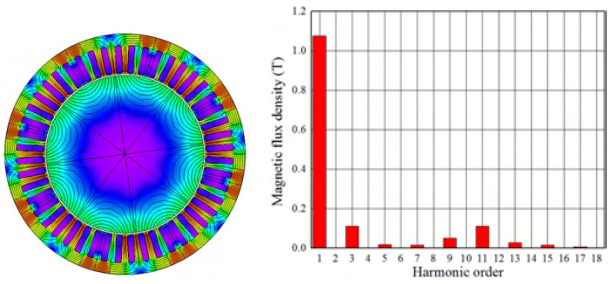


(a) Magnetic flux density and flux lines. (b) Harmonic contents.

Fig. 5. Magnetic flux density and harmonic contents of solid inner-rotor without modulator.

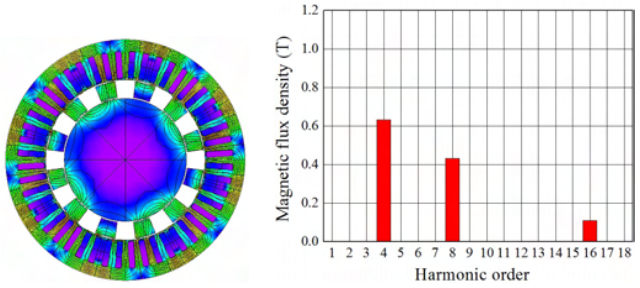


(a) Magnetic flux density and flux lines. (b) Harmonic contents.

Fig. 6. Magnetic flux density and harmonic contents of solid inner-rotor without modulator.

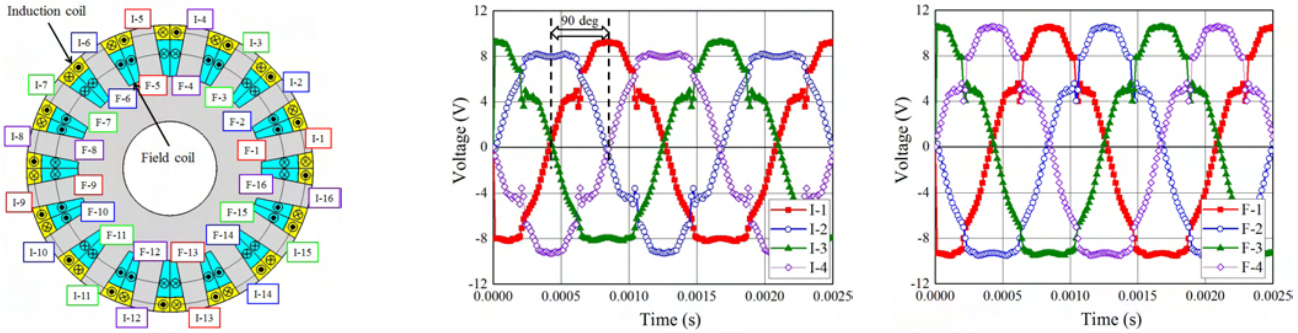


(a) Wound-field rotor. (b) Induced voltage in induction coil I-1, I-2, I-3 and I-4. (c) Induced voltage in field coil F-1, F-2, F-3 and F-4.

Fig. 7. Induced voltage in opened rotor windings of proposed wound-field inner rotor.

$$P_m\omega_m - P_{pm}\omega_{pm} = P_s\omega_s . \quad (7)$$

In addition, without considering the power losses occurred in the proposed motor, it yields:

$$T_s = -\frac{P_s}{P_m}T_m = \frac{P_s}{P_{pm}}T_{pm} \quad (8)$$

where $T_s$ is the stator reaction torque, $T_m$ is the modulator torque, $T_{pm}$ is the PM-rotor torque. The first term of Eq. (3) indicates that the magnetic flux variation of differencial frequency between rotating magnetic field of the stator and the rotor rotation speed links to rotor. Therefore, the eddy current of PMs will extremely occur due to the large variation of the magnetic flux density distribution in air gaps. It consequently occurs in operation principle of the magnetic geared motor using pole pieces (modulator), which generates the magnetic flux permeance distribution in air gaps. As a results, operating point of magnetic flux density in magnet extremely changes by an opposing magnetic field with respect to magnet permeance changes as shown in Fig. 3. In this figure, the red lines shows demagnetization curve at 170 degrees Celsius of Nd-Fe-B ($B_r$ = 1.22 T, $H_{cb}$ = 965.7 kA/m @ 20 degree Celsius / $B_r$ =1.05 T, $H_{cb}$ = 602 kA/m @ 170 degree Celsius ) and black line shows operating point of magnetic flux density in magnet under the opposing magnetic field, which is under the operating condition in Fig. 4. Because the permeance of the magnet greatly changes by the differencial frequency magnetic flux, it is demand that a high coercivity magnet is used for magnetic geared motor.

### B. *Differencial Frequency Linking to inner-rotor*

To solve the drawback of the conventional PM-type magnetic geared motor, a novel self-excited wound-field magnetic geared motor is proposed in this paper. The wound-field rotor that replace the PMs with electromagnet coil are consist of self-excited technology applied diode rectifier circuit utilizing the magnetic flux variation in the asynchronous frequency as replacement of the expensive magnet. Actually, the proposed motor can utilize the magnetic flux variation in differencial frequency between stator rotating magnetic field and rotor rotation speed (diffirencial frequency magnetic flux), which was the drawback to increase the iron loss in the conventional PM-type magnetic geared motor. Figure 5 and Fig. 6 shows magnetic flux density distribution, flux lines and its harmonic contents of distributed winding stator and solid inner-rotor with or without modulator (outer-rotor) in a 4 pole-pair stator and a 12 pole modulator. These results are simulated in the operating condition of Fig. 4. As can be seen in Fig. 5 and Fig. 6, it can be confirmed that the magnetic fluxes of the armature winding in fundamental frequency is modulated by the modulator as indicated in Eq. (3). In addition, it can be confirmed that the eighth rotating magnetic field and sixteenth rotating magnetic field, i.e., eighth space harmonic and sixteenth space harmonic, which is generated by the slot combination between the stator pole-pair and modulator pole as expressed by Eq. (3). Therefore, the number of pole pair of inner rotor should be selected eight according to Eq. (7). On the other hand, the fourth rotating magnetic field in Fig. 6 (b) is the stator fundamental rotating magnetic field, which link to

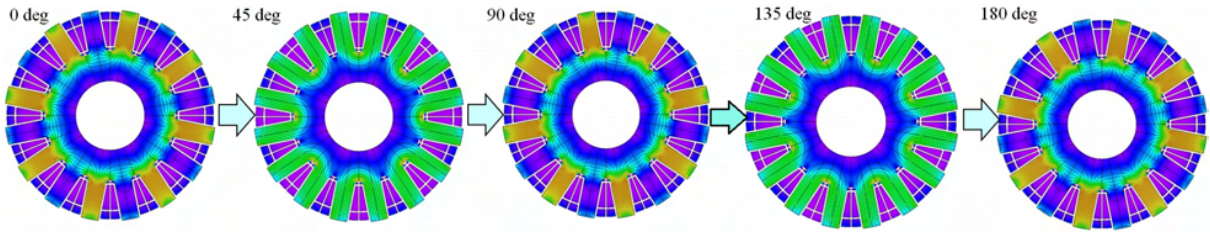


Fig. 8. Magnetic flux density and flux lines of differencial frequency flux with respect to rotor angle.

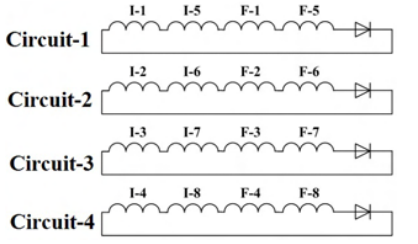


(a) Rotor windings.

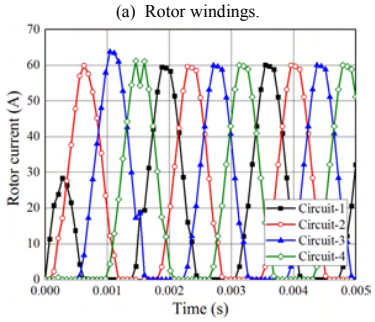


(b) Rotor current.

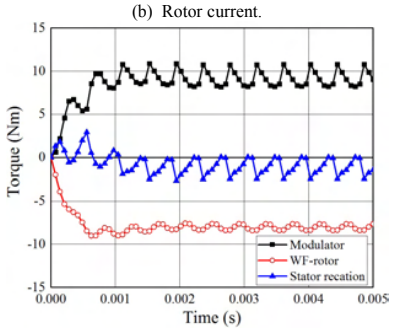


(c) Torque characteristics.

Fig. 9. Torque characteristics and rotor current waveforms under stator 400 Hz and rotor 200Hz of half-bridge rectifier.

inner-rotor without being modulated by the permeance distribution of the modulator. The proposed motor is able to utilize inherent dissipated power energy from the differencial frequency flux which linked to rotor by applying a electromagnetic induction principle of induction machine and a diode rectification technique of self-excitation.

## III. Study on Rotor Winding Rectifying Circuit

Figure 7 (a) shows the proposed wound-field inner-rotor. Fig. 7 (b) and (c) shows the induced voltage waveforms of each coils in Fig. 7 (a), where I and F indicates two types of winding, i.e., an induction coil that retrieves mainly the differencial frequency magnetic flux and an field coil for the field magnetization. This induced voltage is mainly caused by the linkage of the differencial frequency magnetic flux, i.e., the fourth rotating magnetic field in Fig. 6 (b). Figure 7 (b) and (c) illustrate only the induced voltage form the I-1 to the I-4 to become the symmetry at mechanical angle 90 deg in a period. For example, I-1 and I-5, I-9, I-13 become the same wave pattern. As can be seen in Fig. 7 (b) and (c), the phase difference of the coil next to each other becomes 90 deg in electric angle, since the differencial frequency flux (fourth rotating magnetic field) becomes one period in mechanical angle 45 deg. Figure 8 shows the magnetic flux density and flux lines of differencial frequency magnetic flux linking to inner-rotor with respect to rotor angle. As can be seen in Fig. 8, the differencial frequency magnetic flux link to rotor coil in orthogonal direction and it is necessary to consider that induced voltage occurs in all coils wound on salient poles.

### A. Half-Bridge Rectifying Circuit

As shown in Fig. 9, every rotor coil is connected in series in a group with the same voltage phase pair for utilizing induced magnetmotive force in induction coil (I-coil) and the field coil (F-coil), effectively. The rotor winding rectifying circuit of from I-1 to I-4 is consisted of four series connected coils to reduce rotor copper loss and composed four segmented diode rectifying circuits. Figure 9 (a) and (b) shows rotor current waveforms and torque characteristics in operating condition of Fig. 4. Here, it is simulated under the condition of the armature current is 150 $A_{rms}$ and the current phase is the maximum point of electromagnet torque. As shown in Fig. 9, the torque ripple is low to vary in the timing when a field current is zero in each rotor rectifying circuit. However, the output torque per rotor current ratio is low and it need to choose the diode of high $I_F$ characteristics. In addition, the number of the diodes increases more.

### B. Full-Bridge Rectifying Circuit with Common Mode of I-Coil in Forward Direction and F-Coil

As shown in Fig. 10, the I-coil pair of the reverse phase is connected in forward direction and reverse direction to a common cathode diode module. In addition, the F-coil is connected to cathode to be the common mode with the I-coil in forward direction. Figure 10 (b) and (c) shows the FE analysis results simulated in the drive condition same as III-A section. As shown in these figure, an induced current of I-coil in forward direction and F-coil occurs due to the common mode pair, however, the I-coil in reverse direction does not flow the induced current due to the magnetic interference. To make

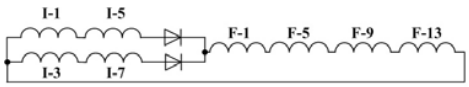


(a) Rotor windings.

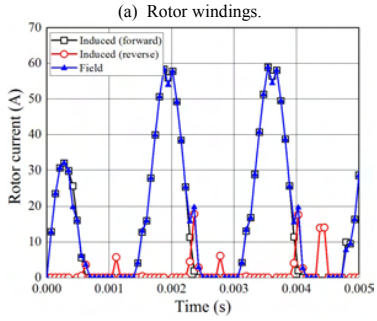


(b) Rotor current.

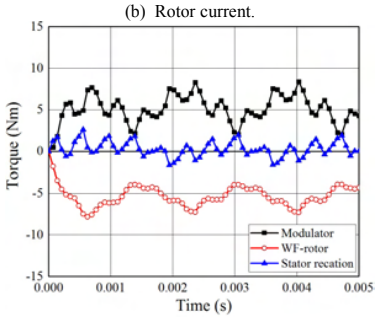


(c) Torque characteristics.

Fig. 10. Torque characteristics and rotor current waveforms under stator 400 Hz and rotor 200Hz of full-bridge rectifier with common mode of I-coil in forward direction and F-coil.

matters worse, for the large field current ripple that is almost half-bridge rectifier, the torque ripple largely increase.

### C. *Full-Bridge Rectifying Circuit with Decoupling between I-Coil and F-Coil*

As shown in Fig. 11, the I-coil pair of the reverse phase is connected in forward direction and reverse direction to a common cathode diode module. In addition, the F-coil is connected to cathode to be the coil pair which can cancel the induced voltage in F-coil pair. According to the study in previous section, it is found that the decoupling between I-coil and F-coil can improve the output torque per rotor current ratio and torque ripple reduction. To accomplish this, it is necessary to select the F-coil pair which the induced voltage ca be canceled. Thus, the induction coil is exclusively used to retrieve field magnetization generator and the field coil is for the field magnetization, i.e., electromagnet coil. Figure 11 (b) and (c) shows the FE analysis results simulated in the drive condition same as III-A section. By referring to rotor current waveforms and torque characteristics in these figure, it can be confirmed that rotor current is performed full-bridge rectifier and the highest output torque per rotor current ratio compared with other rotor winding connection pattern. In addition, it can be realize low torque ripple characteristics.

## IV. Balance Desigen of Rotor Electromotive Force

Figure 12 shows the cross section of proposed permanent-magnet-free magnetic geared motor. The rotor windings

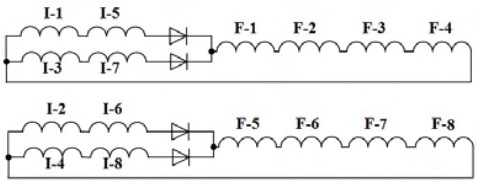


(a) Rotor windings.

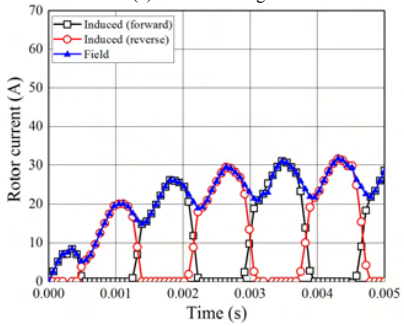


(b) Rotor current.

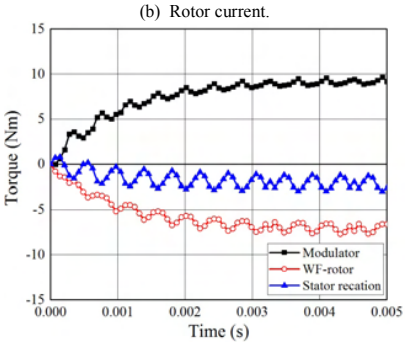


(c) Torque characteristics.

Fig. 11. Torque characteristics and rotor current waveforms under stator 400 Hz and rotor 200Hz of full-bridge rectifier with common mode of I-coil in forward direction and F-coil.

wound on the salient pole of inner-rotor is connected as shown in Fig. 11 (a). Pole combination is $P_s = 4$ , $P_{pm} = 8$, $P_m = 12$.

In this chapter, the technique of rotor magnetomotive force design is explained by regulating coil-turn balance of I-coil and F-coil. Figure 13 shows the rotor winding space factor in the case of I-coil turn number is 10 and F-coil turn number is 11 as an example. As a result of insulation designs such as insulator bobbin and motor size of prototype machine for operation principle inspection, rotor winding of 21 coil-turn in the sum of I-coil and F-coil per one pole can be wound on inner-rotor. Figure 14 shows the modulator torque and magnetomotive force on each rotor coils with respect to number of I-coil turn which is simulated in the drive condition same as III-A section. As can be seen in this figure, it can guess that the most suitable ratio for distribution of I-coil and F-coil exists. Then, the frequency-dependent characteristics of the magnetomotive force balance between the I-coil and F-coil are inspected by FE analysis. Figure 15 shows the modulator torque and average induced current with respect to number of I-coil and differencial frequency. As shown in Fig. 15 (a), it can be confirmed that the maximum torque point has the frequency dependence of magnetomotive force balance between the I-coil

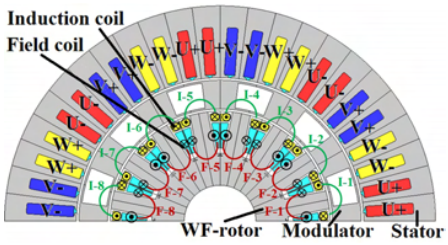


Fig. 12. Cross section of proposed motor.

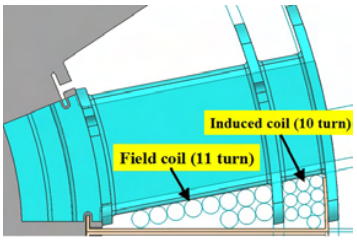


Fig. 13. Rotor winding space factor.

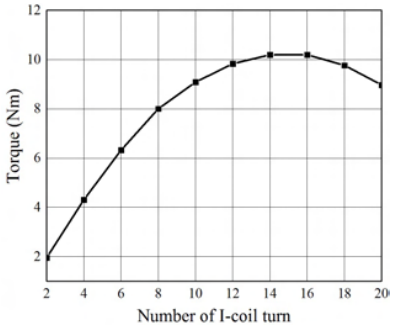


(a) Modulator torque with respect to number of I-coil turn.

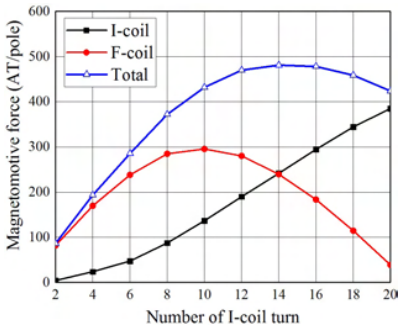


(b) Magnetomotive force with respect to number of I-coil turn.

Fig. 14. Modulator torque and magnetomotive force with respect to number of I-coil turn.

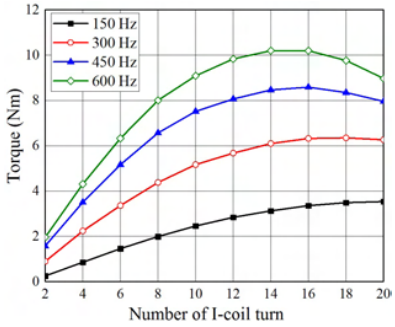


(a) Modulator torque.

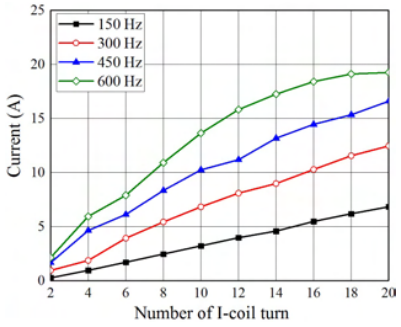


(b) Induced current (average).

Fig. 15. Modulator torque and average induced current with respect to number of I-coil turn and differencial frequency.

and F-coil. And, it can be confirmed that the rotor induced current characteristics changes by the number of the turn ratio between I-coil and F-coil and differencial frequency. In the prototype design, the number of rotor coil is selected as I-coil is 10 T, F-coil is 11 T from the limitation of the rotor current density.

## V. Mechanical Design of Prototype and Drive Performance Prediction

### A. Mechanical Design

The overall structure of the prototype machine which contain a modulator (outer-rotor) and a wound-field rotor (inner-rotor ) in the stator, and both rotor can be driven independently as shown in Fig. 16 (a). Each positional information of the modulator and the wound-field rotor (WF-rotor ) can be acquired by using resolver. And, these rotors are controlled by synchronizing the angular velocity of the armature current which is calculated by Eq. (7). Figure 16 (b) shows the modulator structure with the PPS resin bar contained in the cavity area between pole piece and this resin bar plays a role in transmitting the torque. Furthermore, each material is adjusted the concentricity by spigot joint portion structure. Figure 16 (c) shows the WF-rotor structure and the diode module is mounted on the rotor coil end cover. The specifications of the motor are listed in Table I.

### B. Adjustable Speed Drive Performance in HEV Mode by FE-Analysis

The proposed motor is applied for HEV application as shown in Fig. 1(b), i.e., the modulator is connected to drive shaft, and the WF-rotor is connected to Engine output shaft. The reciprocating engine for compact car can be driven from 3000 r/min to 4000 r/min, efficiently. In addition, the combustion efficiency decrease over 5000 r/min, extremely. In proposed HEV system, the maximum engine speed is limited under 5000 r/min for system efficiency. Figure 17 shows the modulator speed - modulator torque characteristics with respect

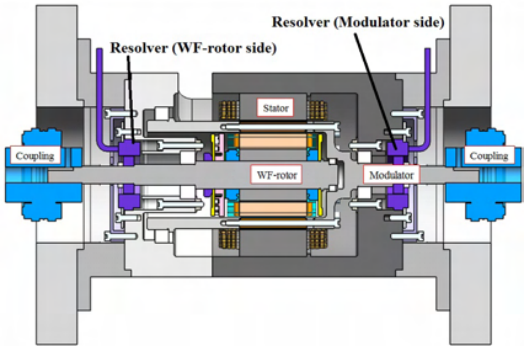


(a) Mechanical configuration (cross section).

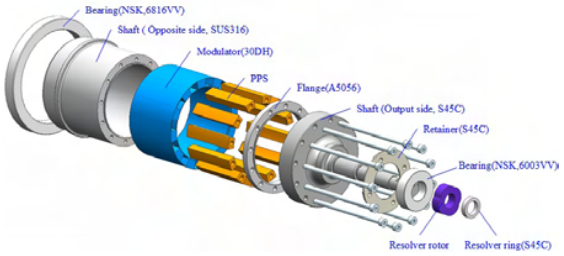


(b) Mechanical configuration of modulator.

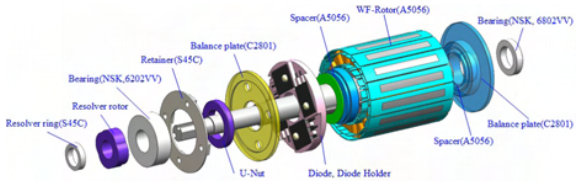


(c) Mechanical configuration of WF-rotor.

Fig. 16. Mechanical design of prototype.

TABLE I. SPECIFICATIONS OF PROPOSED MOTOR

| | |
|---|---|
| Number of stator poles | 8 |
| Number of rotor poles | 16 |
| Number of modulator poles | 12 |
| Stator outer diameter | 120 mm |
| Rotor diameter | 61.2 mm |
| Axial length of core | 49.5 mm |
| Air gap length | 0.7 mm |
| Maximum current | 150 $A_{rms}$ |
| Armature winding resistance | 15.1 mΩ / phase |
| Number of armature coil-turn | 8 |
| Winding connection | 4 series - 2 parallel |
| Number of I-coil turn | 10 |
| Number of F-coil turn | 11 |
| I-coil resistance | 79 mΩ / pole |
| F-coil resistance | 47 mΩ / pole |
| Thickness of iron core steel plate | 0.3 mm (30DH) |

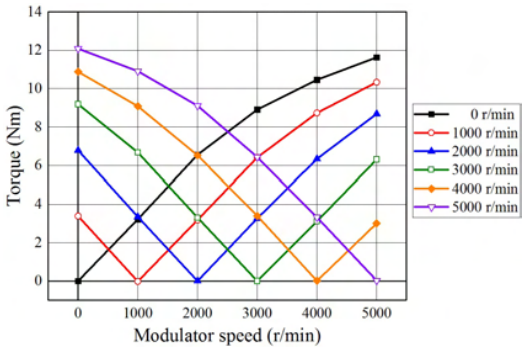


Fig. 17. Modulator speed-torque characteristics with respect to engine speed.

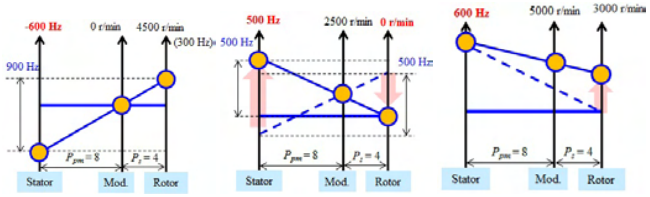


Fig. 18. HEV drive mode with respect to stator excitation frequency and engine speed.

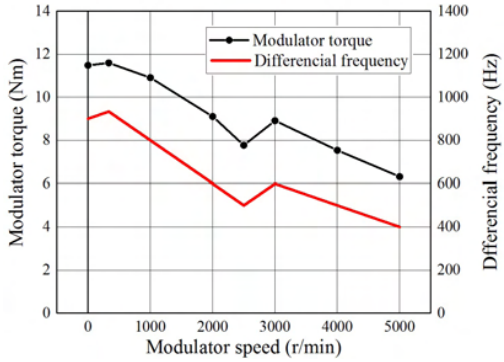


(a) Maximum modulator torque characteristics.

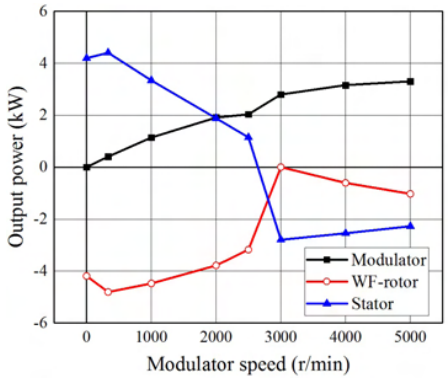


(b) Output power characteristics under maximum torque control.

Fig. 19. HEV driving mode under maximum output torque control.

to engine speed under the condition that the engine speed is controlled in the range of to 5000 r/min from 0 r/min. The synchronized frequency of stator magnetic field and the rotor rotation speed varies according to engine speed from the collinear chart relationship as shown in Fig. 2. Under the

synchronizing mode, the electromagnet torque does not occur because the induced voltage on the WF-rotor can not obtained. However, the differencial frequency can be generated by controlling the speed and torque of WF-rotor, i.e., the engine speed control in HEV mode can be increase output torque. Here, the maximum output torque control by WF-rotor speed control, i.e., engine speed control is considered in various HEV drive mode as shown in Fig. 18. As a study condition, the upper limit of the variable frequency range of the stator rotating magnetic field is 600 Hz. It is because that the carrier frequency of inverter is set on 12 kHz, and depends on the frequency band, which can control stably. Under these limitation, the HEV mode is selected with maximum differencial frequency control. Figure 19 (a) shows the maximum modulator torque control characteristics. As shown in Fig. 19 (a), the output torque can increase with the differencial frequency generation by controlling the engine speed. Fig. 19 (b) shows the output power characteristics under maximum output torque control. In the low modulator speed area, where the differencial frequency is high, the input power from the WF-rotor (engine output power) is regenerated by stator. On the other hand, in the high modulator speed area, where the differencial frequency is low, the input power from the engine and stator becomes the modulator output power.

## VI. Conclusion

This paper has presented a newly permanent-magnet-free magnetic geared motor where the differencial frequency magnetic flux between the stator rotating magnetic field and WF-rotor rotation speed is utilized for field magnetization instead of permanent magnets. The operating principle has analytically discussed. In addition, it has clarified that the relations between the output torque and the rotor coil design for rotor magnetomotive force generation. Furthermore, the prototype design for operating principle inspection has been revealed and its drive performance in HEV mode has been investigated by FE analysis. The future work of the study is to verify the theoretical discussion and the analysis results through experimental tests. Figure 20 shows the actual prototype motor. It is also important to develop the mathematical model since estimation of the induced current and the field current of the rotor windings is significantly important for the proposed motor.

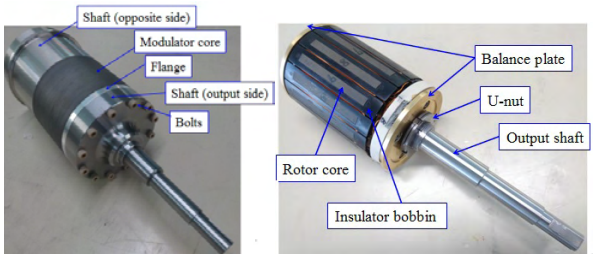


(a) Modulator. (b) WF-rotor.

Fig. 20. Actual prototype machine.

## References


[1] Y. Daisho : "Prospect on Environmental and Energy Vehicle Technologies", *NTN Technical Review (contributed paper),* No. 79, pp.2-11 (2011) (in Japanese)

[2] R. Mizutani : "Technical Feature and Subjects of Traction Motors for EV/HEV", *IEEJ Techinical Meeting*, VT-13-026 (2013) (in Japanese)

[3] M. Kamiya : "Development of Traction Drive Motors for the Toyta Hybrid System", *IEEJ Trans. IA*., Vol. 126-D, No. 4, pp.473-479 (2006) (in Japanese)

[4] Y. Sato, S. Ishikawa, T. Okubo, M. Abe and K. Tamai : "Development of High Response Motor and Inveter System for the Nissan LEAF Electric Vehicle", *SAE Technical Paper*, No. 2011-01-0350 (2011)

[5] Finley, W., Veerkamp. B,. Gehring. D,, and Hanna. P., : "Improving Motor Efficiency Levels Globally", *IEEE IA. Magagine*, vol. 15, No. 1, pp. 39-49 January/February (2009)

[6] Toyota HP, http://www.toyota.com/prius/

[7] Chevrolet HP, http://www.chevrolet.com/volt-electric-car.html

[8] Nissan HP, http://www.nissanusa.com/electric-cars/leaf/

[9] Y. Takeuchi, H. Kato, M. Tago, S. Ogasawara and H. Sakai : "Operating Principle and Control Method of the Magnetic Modulated Motor", *IEEJ Annual Meeting*, No. 5-041, pp.73-74 (2013) (in Japanese)

[10] M. Fukuoka, K. Nakamura, H. Kato and O. Ichinokura : "A Consideration of the Optimum Configuration of Flux-Modulated Type Dual-Axis Motor", *IEEJ Technical Meeting*, RM-13-141 (2013) (in Japanese)

[11] N. Niguchi and K Hirata : "A Novel Magnetic-Geared Motor", *Japan Society of Applied Electromagnetics and Machines*, Vol.21, No.2, pp.110-115 (2013) (in Japanese)

[12] H. T. Faus : "Magnet Gearing", U.S. Patent 2,243,555, May 27 (1941)

[13] K. Atallah, S. Calverley and D. Howe : "Design, Analysis and Realization of a High-Performance Magnetic Gear ", *IEEE Proceedings-Electric Power Applications*, Vol. 151, No. 2, pp.135-143 (2004)

[14] C. C. Huang, M. C. Tsai, D. G. Dorrell and B. J. Lin : "Development of a Magnetic Planetary Gearbox ", *IEEE Transactions on Magnetics*, Vol. 44, No. 3, pp.403-412 (2008)

[15] L. Jian and K. T. Chau : "Design and Analysis of of Integrated Halbach-magnetic-geared Permanent-magnet Motor for Electric Vehicle ", *Journal of Asian Electric Vehicles*, Vol. 7, pp. 1213-1219 (2009)

[16] T. Tonari, H. Kato and H. Matsui : "Study on Iron Loss of Flux Modulated Type Dual-Axis Motor ", *IEEJ Technical Meeting*, RM-13-142 (2013) (in Japanese)

[17] L. Jian and K. T. Chau : "Design and Analysis of a Magnetic-Geared Electric-Continuously Variable Transmission System Using Finite Element Method ", *Progress in Electromagnetic Research*, Vol. 7, pp. 47-61 (2010)

[18] S. Nonaka : "The Self-Excited Type Single-Phase Synchronous Motor ", *IEEJ Trans. IA*, Vol. 78, No. 842, pp. 1430-1438 (1958-11) (in Japanese)

[19] M. Aoyama and T. Noguchi : "Torque Performance Improvement with Modified Rotor Winding Circuit of Wound-Field Synchronous Motor Self-Excited by Space Harmonics ", *IEEJ Trans. IA*, Vol. 134, No. 12, pp. 1038-1049 (2015) (in Japanese)

[20] M. Aoyama, Y. Kubota and T. Noguchi : "Study on Rare-Earth-Free Magnetic Geared Motor Self-Excited by Differencial Frequency and Space Harmonics", *IEEJ Annual Meeting*, No. 5-038, pp. 70-71 (2015)